Raman Spectroscopy and Time-resolved Photoluminescence of BN and $B_xC_yN_z$ Nanotubes

J. Wu[1], Wei-Qiang Han[1,2,3], W. Walukiewicz[1], J. W. Ager III[1], W. Shan[1], E. E. Haller[1,4], and A. Zettl[1,2,3]*

1. Materials Sciences Division, Lawrence Berkeley National Laboratory, Berkeley, California 94720

2. Department of Physics, University of California, Berkeley, California 94720

3. Molecular Foundry, Lawrence Berkeley National Laboratory, Berkeley, California 94720

4. Department of Materials Science and Engineering, University of California, Berkeley, California 94720

RECEIVED DATE ( )

We report Raman and time-resolved photoluminescence spectroscopic studies of multi-walled BN and $B_xC_yN_z$ nanotubes. The Raman spectroscopy shows that the as-grown $B_xC_yN_z$ nanotubes are radially phase separated into BN shells and carbon shells. The photoluminescence decay process is characterized by two time constants that are attributed to intra- and inter- BN sheet charge recombination, respectively. Comparison of the photoluminescence of BN nanotubes to that of hexagonal BN is consistent with the existence of a spatially indirect band gap in multi-walled BN nanotubes as predicted by theory.

Hexagonal boron nitride (h-BN) is iso-structural with graphite and is the normal phase of BN that is stable at room temperature and ambient pressure. It is a wide band gap semiconductor with potential applications in optoelectronic devices. First-principles local-density calculations have shown that the lowest band gap (4.07 eV) is indirect, located near the Brillouin-zone edges. However, due to the quasi-two dimensional nature of the hexagonal structure, the lowest direct band gap is predicted to be close by

* Corresponding author, E-mail: W_Walukiewicz@lbl.gov

at 4.2 eV [1]. A wide range of lowest gap energies, such as 3.8 eV [2], 4.3 eV [3], 5.2 eV [4] and 5.9 eV [5], have been reported by experimental studies using various techniques.

When a hexagonal BN sheet is rolled up into a single-walled BN nanotube (NT), its electronic structure is very different from that of carbon nanotubes because of the wide gap of BN sheets as opposed to the zero gap in graphite. In contrast to carbon nanotubes, which have diverse electronic properties depending on their structure, the band gaps of BN NTs are predicted theoretically to be approximately equal to that of h-BN, nearly independent of their radius and chirality, except for a band gap narrowing in thin NTs (diameter < ~ 0.8 nm) as a result of sp^3 (π) hybridization induced by the high curvature [6]. In this context, the predicted structural independence of the electronic properties and thermal stability of BN NTs open promising opportunities for applications in nanoelectronic and nanophotonic devices. The optical properties of BN NTs are still not well understood due to poor sample quality and low light emission efficiency.

Recently, it was demonstrated that multi-walled BN and boron carbon nitride ($B_xC_yN_z$) NTs can be synthesized at large quantities using a carbon nanotube substituted reaction [7]. Transmission Electron Microscopy (TEM) shows that high-quality, nearly-perfect layer-structured BN or $B_xC_yN_z$ NTs can be grown in either individual or bundled form. In this letter we present results of optical spectroscopy studies of such BN and $B_xC_yN_z$ NTs. Raman spectroscopy and continuous-wave and time-resolved photoluminescence have been carried out, and results are compared to recent theoretical calculations.

$B_xC_yN_z$ nanotubes were synthesized via the carbon nanotube-confined reaction using chemical vapor deposition-derived carbon NTs together with B_2O_3 and N_2 at 1600^{o}C for half an hour. Subsequent thermal oxidation treatment at 650 ^{o}C transformed efficiently the $B_xC_yN_z$ NTs into BN NTs. Details of sample synthesis and oxidation processes have been published elsewhere [7]. The resulting product is a mixture of 60-70% multi-walled $B_xC_yN_z$ (or BN after oxidation) NTs and ~ 30-40% $B_xC_yN_z$ (or BN) fullerene-like particles (mostly), nanoparticles, and nanowires. Electron Energy Loss Spectroscopy (EELS) shows that, prior to oxidation, the C/B atomic ratio is between 0.2 and 0.4, and after oxidation it is reduced to < 0.02. Most NTs have outer diameters below ~ 8 nm and about 2 to 8 walls, as

demonstrated by the high-resolution TEM images shown in Fig. 1 (a) and (b). After the removal of carbon by oxidation from the $B_xC_yN_z$ NTs, the average number of the NT layers is reduced and the walls of the NTs still appear to be free of large defects, suggesting that the original $B_xC_yN_z$ NTs are radially phase separated into BN shells and carbon shells. Similar results were reported by Suenaga *et al.* on $B_xC_yN_z$ NTs made by the arc-discharge method [8].

The Raman scattering spectra were excited with a frequency-doubled (244 nm) Argon laser and recorded by a liquid-nitrogen cooled CCD camera. The continuous-wave photoluminescence (PL) spectra were generated in the backscattering geometry by excitation with the same laser and were detected by a photomultiplier tube. The time-resolved PL was excited with 200-fs pulses from a frequency-tripled (267 nm) mode-locked Ti : sapphire laser, dispersed with a 0.25-m single-grating monochromator, and detected with a synchroscan streak camera. The system spectral and temporal resolution were 0.05 nm and 11 ps, respectively. For all the experiments, commercial hexagonal BN powder (grain size ~ several μm, see Fig.1 (c)) was also measured as a comparison. All experiments were performed at room temperature.

Figure 2 shows the Raman spectra of h-BN, $B_xC_yN_z$ and BN NTs in the wavenumber range of interest. The dominant peak near 1366 cm^{-1} that shows up intensely in all three samples is attributed to the well-known zone-center, counter-phase B-N vibrational mode (E_{2g}) within BN sheets [4, 9]. As shown in the inset of Fig. 1, this E_{2g} mode is broadened and shifted to higher wavenumber in the BN and $B_xC_yN_z$ NTs. The peak shift is about 2.1 cm^{-1} and the full width at half maximum (FWHM) increases from 15.6 cm^{-1} in h-BN to 17.9 cm^{-1} in the BN and $B_xC_yN_z$ NTs. Nemanich *et al.* have reported a correlation between the width and peak energy of this mode and the average crystal grain size of the h-BN sample [10]. The shift and broadening were explained in a formulation of the Raman cross section for scattering from nanocrystals in which the wave-vector uncertainty of the phonons is related to the crystal grain size. The shift of this peak from its bulk value can be described by $380\times10^{-8}/L$ - 0.29 cm^{-1} and its FWHM by $1417\times10^{-8}/L$ + 8.7 cm^{-1}, where L is the average crystal size [10]. From these quantitative relationships we estimate the effective "crystal size" to be ~ 16 nm for our BN and $B_xC_yN_z$ NTs. This

value is close to the average perimeter of the NTs in our sample. The signal may also include contributions from similar-size hexagonally structured nanoparticles.

As compared to the Raman spectrum of BN NTs, the $B_xC_yN_z$ sample shows a strong peak near 1585 cm^{-1} with a FWHM of 48 cm^{-1}. This peak is clearly due to the E_{2g} stretch mode of two-dimensional graphite sheet or carbon shells in the $B_xC_yN_z$ sample [11, 12]. The higher energy of this mode than that of the same mode of BN reflects the softening of the bond as a result of ionicity in BN. The large width may be a result of a superposition of multiple peaks due to differently structured carbon shells, because this mode is chirality and diameter dependent in carbon nanotubes. The emergence of this C-C E_{2g} peak and the absence of any other new peaks associated with B-C or N-C bonds from the $B_xC_yN_z$ sample (as compared to the BN sample) confirms the conclusion drawn from the TEM studies that the $B_xC_yN_z$ NTs are structured in the form of concentric, radially separated BN shells and carbon shells. The fact that the carbon shells do not survive the oxidation process indicates that the majority of them form the outer or the inner layers of the multi-walled structure, rather than being sandwiched between BN shells.

There are also some further weaker peaks in the spectra. A broad peak appears at 920 cm^{-1} for all three samples. Since in perfect h-BN crystal, the only other Raman active mode (in-phase E_{2g} mode) is located far away (near 50 cm^{-1}) [4], this peak at 920 cm^{-1} is probably due to disorder-induced Raman activity or contamination. A sharp peak is observed near 880cm^{-1} for the $B_xC_yN_z$ and BN NTs. This peak has been reported in studies of BN single-walled NTs [13] but its origin has not been identified.

The room-temperature PL spectra of these samples are shown in Fig. 3. All samples show a wide emission peak between 3.5 and 4.2 eV, tailing off toward low energy. The signal is about 100 times stronger for the h-BN sample than in the other samples. Phonon replica features visible on the broad PL peaks are especially pronounced for the h-BN sample. In the inset of Fig. 3 we plot the peak of each phonon replica against the number of peaks. The slope of the linear dependence is 0.17 eV (1370 cm^{-1}) per phonon, which is close to the zone-center E_{2g} phonon energy of BN sheet.

The extrapolation of the linear dependence in the inset of Fig. 3 leads to a zero-phonon line (ZPL) of 4.07 eV for the h-BN and 4.02 eV for the BN and $B_xC_yN_z$ NTs. This value is close to the direct band

gap (4.2 eV at zero temperature) predicted in Ref. [1]. We have also studied the excitation power dependence of the PL peaks. A linear increase in the emission intensity has been observed for all three samples when the excitation laser power was changed by more than three orders of magnitude (not shown here). The absence of saturation in emission intensity at strong excitation and the zone-center phonon replica feature indicate that the emission is indeed caused by band-to-band optical transitions across the direct band gap in the samples.

Both the BN NT and the $B_xC_yN_z$ NT sample appear to be white in general, but large, darker grains (size ~0.5 mm) are visible to the naked eye in the $B_xC_yN_z$ sample. When the excitation laser is focused at these darker grains, the sample exhibits a stronger carbon E_{2g} Raman peak, and a much weaker PL peak as shown by the dashed curve in Fig. 3. Therefore, it can be concluded that the $B_xC_yN_z$ NT sample is inhomogeneous and the darker areas contain more carbon.

Due to the chirality-independent band gap of single-walled BN nanotubes and the weaker coupling between adjacent BN shells, the electronic structure of multi-walled BN nanotubes should be also less diverse than that of multi-walled carbon NTs. However, the σ-π hybridization in high-curvature BN shells that reduces the band gap of small-diameter single-walled BN NTs also plays an important role in multi-walled BN NTs. Local-Density Approximation calculations by Okada *et al.* have shown that in double-walled BN NTs, both the conduction and valence bands of the inner shell with larger curvature are negatively shifted (type-II offset) from those of the smaller-curvature outer shell as a result of their stronger hybridization with remote σ bands [14]. Consequently, in the double-walled structure a spatially indirect band gap is developed, in which the conduction band minimum is located on the inner shell and the valence band maximum is on the outer shell. The fundamental band gap is thus smaller than that of the inner shell by an amount equal to the band offset. For example, the band gap of (5,0), (7,0), (9,0) and (15,0) single-walled BN NTs is calculated to be 2.4, 3.4, 3.8 and 4.4 eV respectively. When these NTs are encapsulated in a (15,0) BN shell, the band gaps are reduced to 1.7 eV for (5,0)@(15,0), 2.9 eV for (7,0)@(15,0), and 3.6 eV for (9,0)@(15,0). The effect is weaker for larger-diameter NTs. The slight downward shift (~ 50meV) of the ZFL in Fig. 3 from h-BN to BN NTs could

be caused by these curvature-induced effects in the multi-walled NTs. The shift is weak which could be due to the large diameter of the NTs in our sample: the maximum outer-shell diameter of ~ 8 nm corresponds to a (90, 0) zigzag NT or a (50, 50) armchair one.

To study the recombination mechanism of the emission, we have carried out time-resolved PL by excitation with a laser line at 267 nm. Figure 4 (a) shows the PL decay profile of the BN NTs at wavelengths 315 nm (3.94 eV), 335 nm (3.70 eV) and 355 nm (3.49 eV). These spectra can be well fit by a double exponential decay function over the entire time range of detection (~ 2 ns). The PL decay process is characterized by a fast decay at the beginning with a time constant of τ_1 ~ 200 ps followed by a slower decay with τ_2 > ~ 1500 ps. In Fig. 4 (b) the two lifetimes obtained are plotted as a function of the emission energy. It can be seen that both lifetimes increase on the lower energy shoulder of the PL peak. This is typical band-edge luminescence behavior in which the shorter lifetime of higher-energy carriers is attributed to the additional relaxation channel via thermalization to lower-energy states [15]. The temporal behavior of the emission from the $B_xC_yN_z$ NTs is quantitatively similar to that of the BN NTs (not shown here).

As a comparison, Fig. 5 shows the lifetime plot of the h-BN sample. The plot shows a qualitatively similar behavior but with several differences. The lifetime τ_2 is longer in the BN NTs than in the h-BN sample by more than 50% in the main peak region. This effect is tentatively attributed to the spatially indirect nature of the band gap in the multi-walled BN NTs. Similar to type-II offset planar quantum wells, the recombination probability of electrons and holes is reduced as a result of the spatial separation of their wavefunction, which increases the lifetime of the PL. On the other hand, the lifetime τ_1, is shorter (by 40%) in the BN NTs. Therefore, it could be speculated that the decay processes associated with the lifetimes τ_1 and τ_2 involve recombination within single BN shells/sheets and between different BN shells/sheets, respectively. As the h-BN sheets form multi-walled NTs, τ_1 is reduced because point defects induced on BN shells act as additional recombination centers. The lifetime τ_2 is increased as a result of the spatial separation of electrons and holes. In both the BN NTs and the h-BN samples, the intensity of the τ_1-related emission is larger by a factor of 5~10 than the τ_2-

related emission. This indicates that the charge relaxation and recombination processes are predominantly occurring within individual hexagonal BN shells in the multi-walled NT structure. This behavior is consistent with the recent observation of strongly delocalized π plasmons along the tube axis in multi-walled BN NTs as studied by EELS [16].

In summary, we have observed strong photoluminescence of multi-walled BN and $B_xC_yN_z$ nanotubes at room temperature. Temporal analysis of the PL signals reveals a charge recombination process dominated by the fast recombination occurring within individual BN sheets. The slower decay process is attributed to the charge transfer and recombination across different BN sheets, and shows a behavior consistent with the predicted spatially indirect band gap of multi-walled BN NTs. Results of Raman Spectroscopy confirm that the multi-walled $B_xC_yN_z$ NTs are structured into radially phase separated BN and carbon shells.

This work is supported by the Director, Office of Science, Office of Basic Energy Sciences, Division of Materials Sciences and Engineering, of the U.S. Department of Energy under Contract No. DE-AC03-76SF00098. W. -Q. H . and A. Z. acknowledge support from the Molecular Foundry, LBNL.

Supporting Information Available.

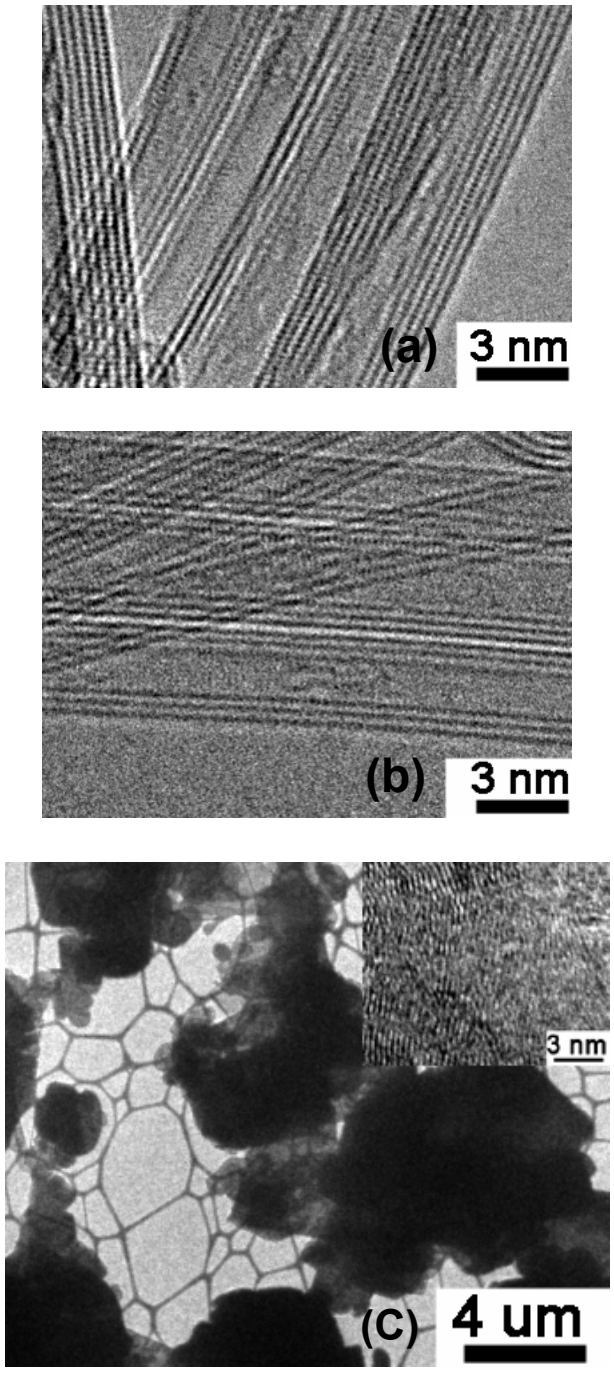

Figure 1. TEM image of (a) $B_xC_yN_z$ nanotubes, (b) BN nanotubes and (c) h-BN powder. Inset is the high-resolution TEM image.

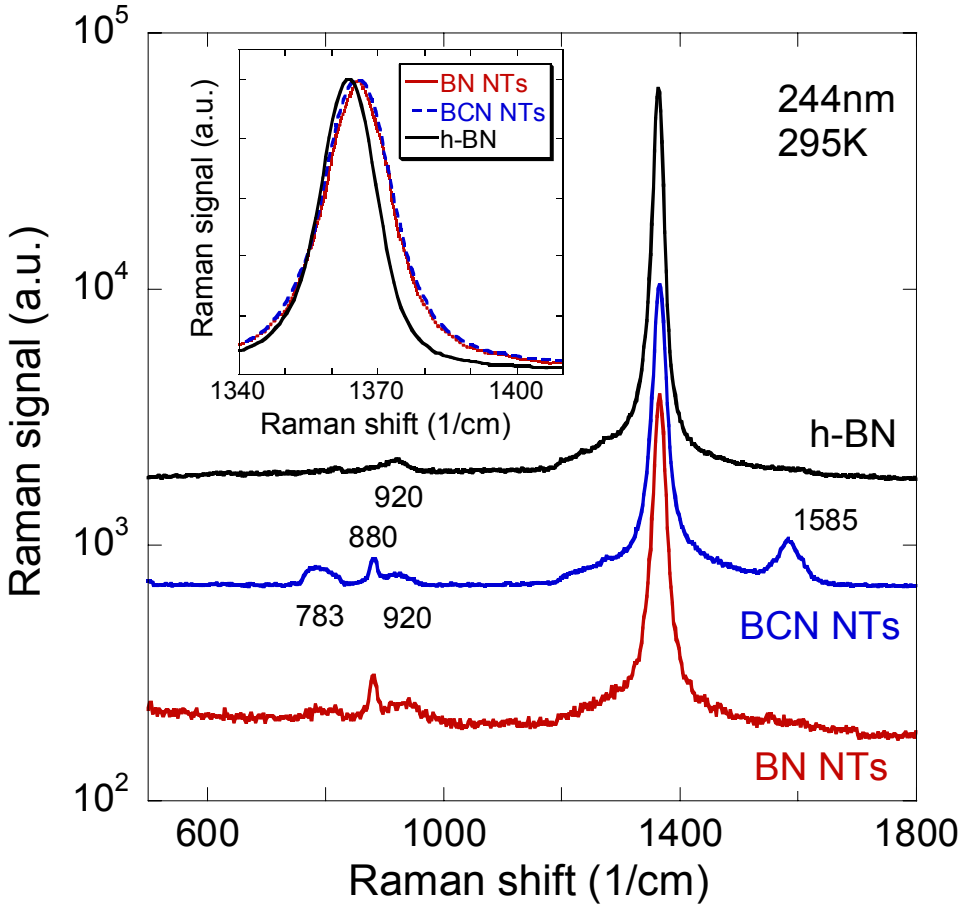

Figure 2. Raman spectra of BN and $B_xC_yN_z$ nanotubes and bulk h-BN recorded at room temperature. Inset shows the main peak near 1366 cm^{-1}.

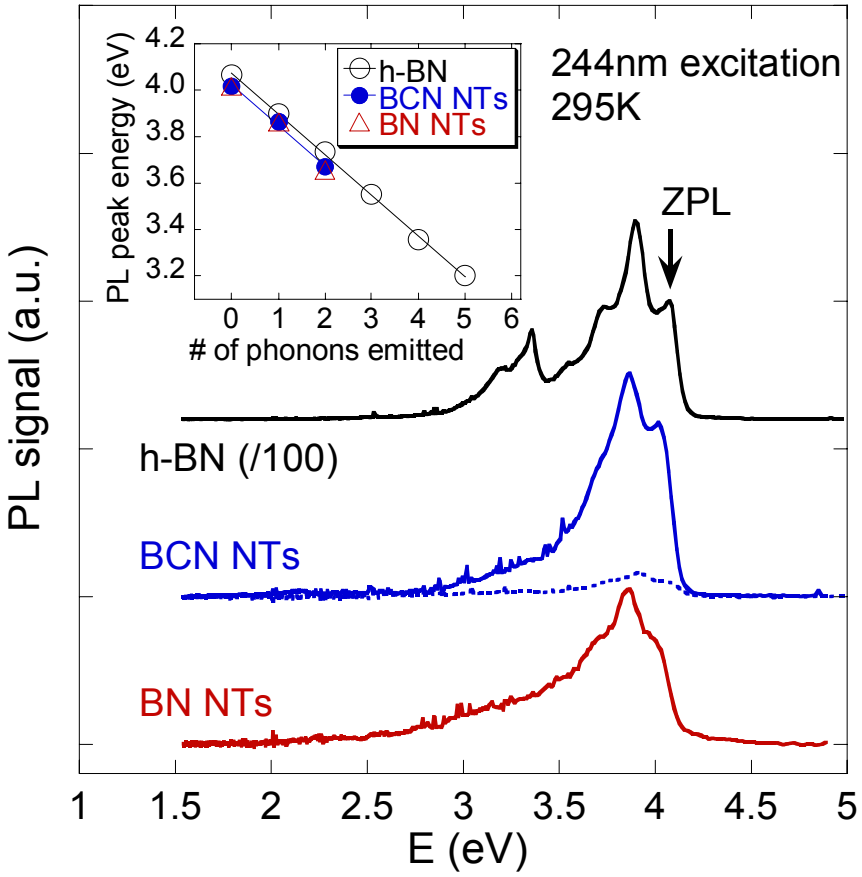

Figure 3. Continuous-wave photoluminescence spectra obtained at room temperature. For the $B_xC_yN_z$ NTs, the dashed curve shows the spectrum recorded when the excitation laser was focused at a dark grain in the sample. The inset shows the phonon replica energies plotted against the number of phonons emitted.

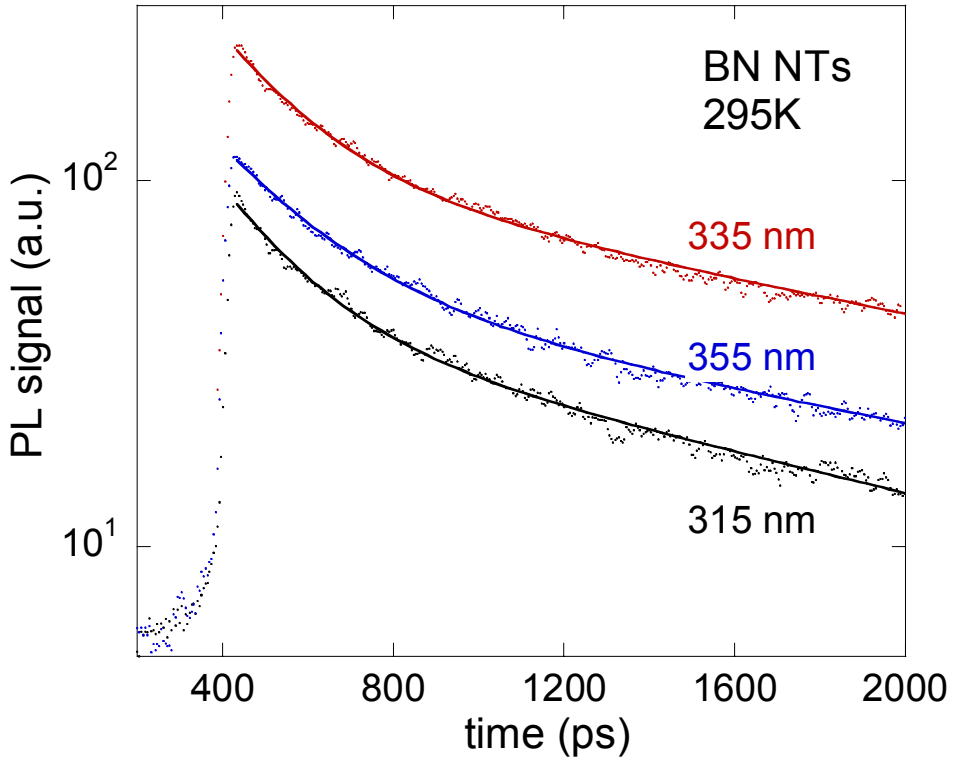
BN NTs
295K
335 nm
355 nm
315 nm
PL signal (a.u.)
10^2
10^1
400
800
1200
1600
2000
time (ps)

(a)

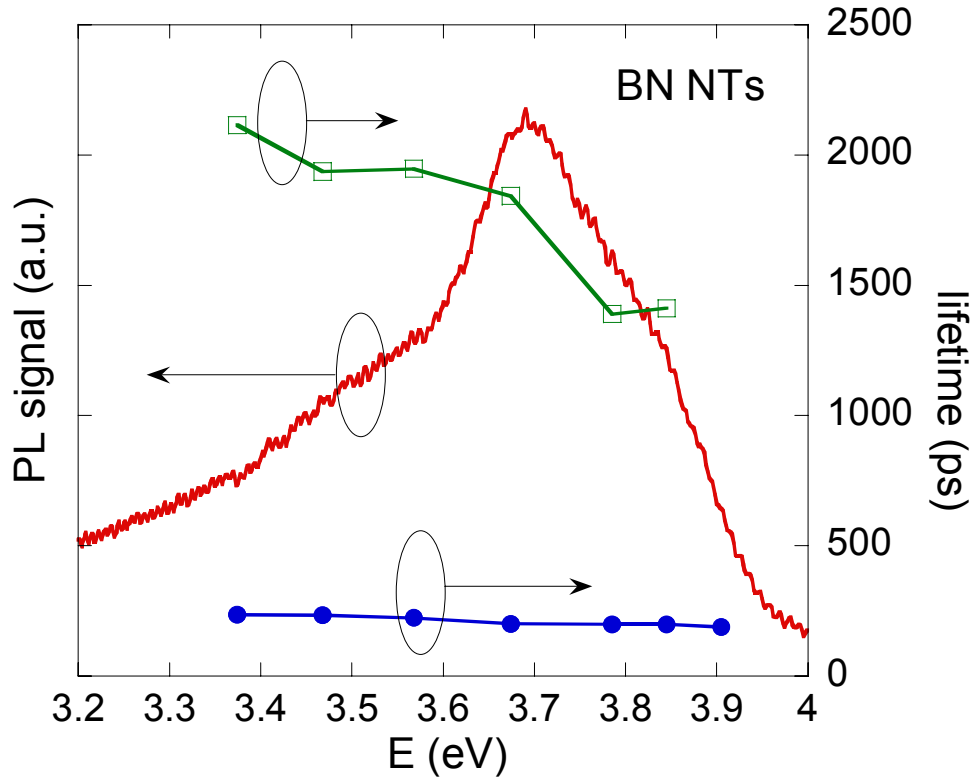
BN NTs
PL signal (a.u.)
lifetime (ps)
2500
2000
1500
1000
500
0
3.2
3.3
3.4
3.5
3.6
3.7
3.8
3.9
4
E (eV)

(b)

Figure 4. (a) Time-resolved photoluminescence of BN NTs. The wavelength window for each curve is 5 nm. The solid curves show the best fit using a double exponential function. (b) The lifetimes obtained from the fitting with the double exponential decay function.

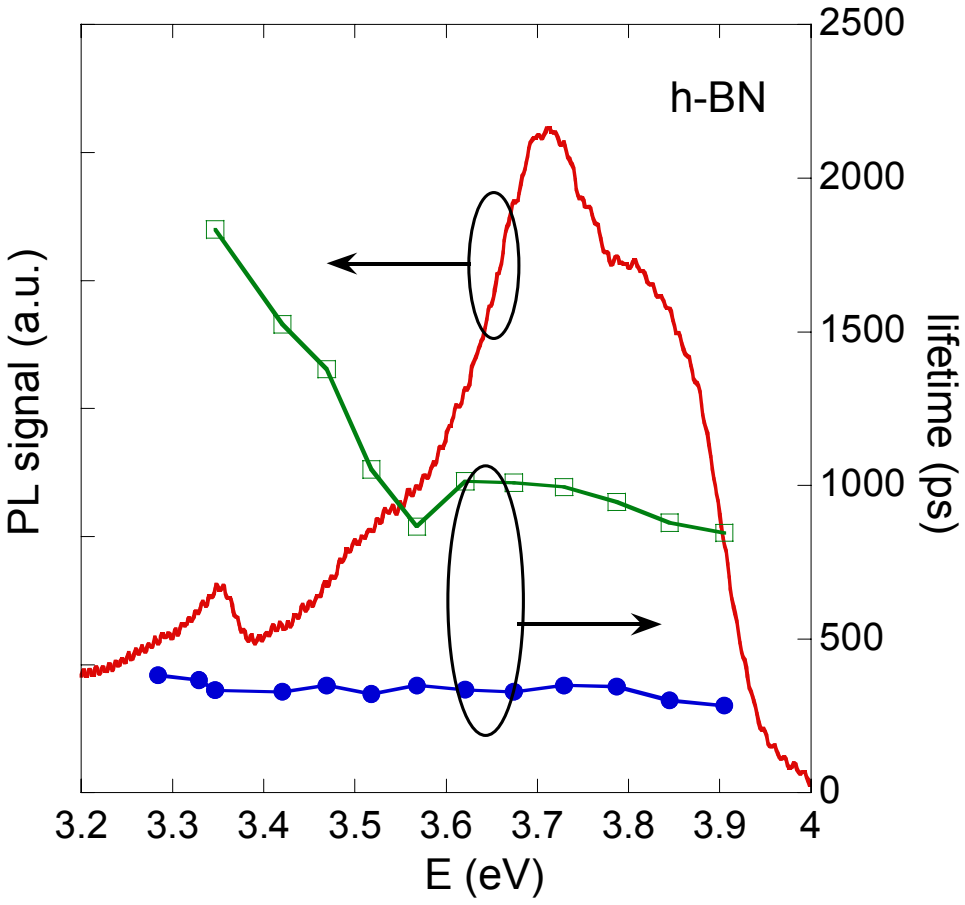

Figure 5. Lifetimes of h-BN obtained from fitting with the double exponential function.

REFERENCES

(1) Xu Y.; Ching, W. Y. *Phys. Rev. B* **1991,** 44, 7787-7798.

(2) Rand M. J.; Roberts, J. F. *J. Electrochem. Soc.* **1968,** 115, 423-427.

(3) Zupan J.; Kolar, D. *J. Phys. C* **1972,** 5, 3097-3100.

(4) Hoffman, D.; Doll G.L; Eklund, P. C. *Phys. Rev. B* **1984,** 30, 6051-6056.

(5) Tarrio C.; Schnatterly, S. E. *Phys. Rev. B* **1989,** 40, 7852-7859.

(6) Rubio, A.; Corkill, J. L.; Cohen, M. L. *Phys. Rev. B* **1994,** 49, 5081-5084. Blase, X.; Rubio, A.; Louie, S. G.; Cohen, M. L. *Europhys. Lett.,* **1994,** 28, 335-340.

(7) Han, W. Q.; Mickelson, W.; Cumings, J.; Zettl, A. *Appl. Phys. Lett.,* **2002,** 81, 1110-1112.

(8) Suenaga, K.; Collix, C.; Demoncy, N.; Loiseau, A.; Pascard, H.; Willaime, F. *Science* **1997**, 278, 653-655.

(9) Popov, V. N. *Phys. Rev. B* **2003,** 67, 085408.

(10) Nemanich, R. J.; Solin, S. A.; Martin, R. M. *Phys. Rev. B* **1981,** 23, 6348-6356.

(11) Rao, A. M.; Richter, E.; Bandow, S.; Chase, B.; Eklund, P. C.; Williams, K. A.; Fang, S.; Subbaswamy, K. R.; Menon, M.; Thess, A.; Smalley, R. E.; Dresselhaus, G.; Dresselhaus, M. S. *Science* **1997,** 275, 187-191.

(12) Eklund, P. C.; Holden, J. M.; Jishi, R. A. *Carbon*, **1995,** 33, 959-972.

(13) de la Concha, R. A.; Wirtz, L.; Mevellec, J. Y.; Lefrant, S.; Rubio, A.; Loiseau, A. *AIP Conf. Proc*., **2003,** 685, 384-388.

(14) Okada, S.; Saito, S.; Oshiyama, A. *Phys. Rev. B* **2002,** 65, 165410.

(15) Kim, H. S.; Mair, R. A.; Li, J.; Lin, J. Y.; Jiang, H. X. *Appl. Phys. Lett.* **2000,** 76, 1252-1254.

(16) Fuentes, G. G.; Borowiak-Palen, E.; Pichler, T.; Liu, X.; Graff, A.; Behr, G.; Kalenczuk, R. J.; Knupfer, M.; Fink, J. *Phys. Rev. B* **2003,** 67, 035429.